Case Studies in Thermal Engineering 35 (2022) 101846

Contents lists available at ScienceDirect

Case Studies in Thermal Engineering

journal homepage: www.elsevier.com/locate/csite

LSM and DTM-Pade approximation for the combined impacts of convective and radiative heat transfer on an inclined porous longitudinal fin

Fuzhang Wang [a], R.S. Varun Kumar [b], G. Sowmya [c], Essam Roshdy El-Zahar [d,e], B.C. Prasannakumara [b], M. Ijaz Khan [f], Sami Ullah Khan [g], M.Y. Malik [h], Wei-Feng Xia [i,*]

[a] Nanchang Institute of Technology, Nanchang, 330044, China
[b] Department of Mathematics, Davangere University, Davangere, 577002, Karnataka, India
[c] Department of Mathematics, M S Ramaiah Institute of Technology, Bangalore, 560054, Karnataka, India
[d] Department of Mathematics, College of Science and Humanities in Al-Kharj, Prince Sattam bin Abdulaziz University, P.O. Box 83, Al-Kharj, 11942, Saudi Arabia
[e] Department of Basic Engineering Science, Faculty of Engineering, Menoufia University, Shebin El-Kom, 32511, Egypt
[f] Department of Mathematics and Statistics, Riphah International University I-14, Islamabad, 44000, Pakistan
[g] Department of Mathematics, COMSATS University Islamabad, Sahiwal, 57000, Pakistan
[h] Department of Mathematics, College of Sciences, King Khalid University, Abha, 61413, Saudi Arabia
[i] School of Engineering, Huzhou University, Huzhou, 313000, PR China

ARTICLE INFO

Keywords:
Convective heating phenomenon
Porous space
Heated fin
Least square scheme

ABSTRACT

The novel exploration designates temperature variation through an inclined porous longitudinal fine with convective radiative phenomenon. The Rosseland approximation is considered for the radiation heat exchange. Using non-dimensional terms, the existing system of stated problem is reduced to ordinary form. To resolve the nonlinear ordinary system of heat transfer, the analytical approaches, differential transform method (DTM) with Pade approximant has been workout. Furthermore, simulations are developed to examine the outcomes of convincing flow parameters like radiative-conduction parameter, porosity parameter, and conduction-convection variable on the thermal distribution for different modes of heat transfer like nucleate boiling and radiative heat transfer. The results show that an increase in the conduction-convection variable, porosity variable, and radiation number causes a reduction in the thermal field. On the other hand, augmentation change is appeared due to heat generation constant. The thermal behavior of the fin declines with escalating angle.

* Corresponding author.
E-mail address: xwf212@163.com (W.-F. Xia).

https://doi.org/10.1016/j.csite.2022.101846
Received 24 October 2021; Received in revised form 12 January 2022; Accepted 1 February 2022
Available online 3 February 2022

Nomenclature:

Q	heat generation constant
σ	Stefan–Boltzmann constant
θ	Dimensionless temperature
R_d^*	Radiation-conduction parameter
α	Inclination angle
β_R^*	Rosseland extinction coefficient
P	Fin's perimeter
Nc	Convective–conduction constant
T	Fluid temperature
g	Acceleration due to gravity
φ	Porosity
S_H	Porosity parameter
γ	Internal heat generating rate
K	Permeability
c_p	Specific heat
Ra	Rayleigh number
ν	Kinematic viscosity
ρ	Density of the fin material
Da	Darcy number
W	Fin's width
A_b	cross-sectional area
Nr	Radiation number
h^*	heat transfer coefficient
β	Volumetric expansion index
x	Fin axial distance
L	Fin length
$q^*_{\text{int}}(T)$	Internal heat generation constant
k^*	Thermal conductivity
H_k	Weight functions
X	Fin's length
ε^*	Emissivity

Subscript

∞	Ambient
b	Base
s	Solid
r	Relative quantity
f	Fluid

1. Introduction

The heat transfer is the fluctuated measurement of energy transfer from high to low temperature surface. Heat exchange activity is predicted in a variety of circumstances due to its importance in varied engineering applications including extrusion, welding, crystal growth, and energy production. Heat transfer enhancement is important in these applications, and conduction, convection, and radiation are the main heat transfer mechanisms. The conduction phenomenon is based on the diffusion of heat in stationary fluid or solid surface while the convection process deals with heating transfer from moisture space due to fluid particles movement. The energy transfer occurrence is referred to the boiling phenomenon in extended surfaces, on the other side, is influential in the system of thermal engineering. The boiling phenomenon is the phase transition which results in production of vapor bubbles on a heated space. This operation can occur in a quiescent fluid environment, known as pool boiling, or in a forced-flow environment, known as forced convective boiling. The process of natural convection is transferred of particles from heated zone to saturated materials without appearance of bubbles on body. It is a single-phase convection process with many physical applications. The heat transfer mechanism is effected with the nucleate boiling. Heat transfer liquids like nanoparticles and hybrid nanomaterials are incorporated to attain the impressive heat transfer. As a result, numerous investigators have explored the transportations heating phenomenon near the boundary layer of different geometries [1–10].

An extended surface/fin, on the other side, is used to boost the heat transmission rate between a solid and the surrounding fluid. The heat exchange of fins is essential in a variety of applications, including oil-carrying pipelines, heat exchangers, processing plants,

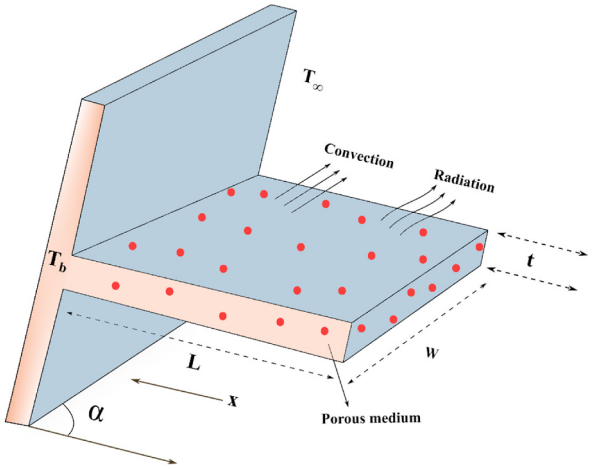

Fig. 1. Schematic of a porous longitudinal fin.

air-cooled turbine blades, and electrical chips. Fins have also been shown to be beneficial in heat-rejection devices in space vehicles and the cooling of electrical parts. Thus, the researchers showed their interest in analyzing the temperature variation in the fins [11–15]. Flow-through porous media is necessary for several thermal engineering applications including filtering, solar collector, insulation, reactor cooling, and inert packed bed reactors. In recent decades, the utilization of porous fins has received much interest.

The physical attribution of this trend is due to superior aspect of porous fine against solid fin with thermal aspect by expanding the available surface area for both convective and radiative energy transmission. Recently, Ndlovu and Moitsheki [16] described the heat transmission and thermal performance of a permeable rectangular fin. Thermal stress features of a porous circular fin with internal heat production were examined by Sowmya and Gireesha [17]. The thermal variation of a permeable fin exposed to convective-radiative energy transmission was inspected by Kundu and Yook [18]. Implementing the differential transformation method (DTM), Sowmya and Gireesha [19] oriented research on heating pattern through diverse structured straight permeable fin. Das and Kundu [20] delineated the impact of the magnetic effect in a circular permeable fin with internally surface heat generation.

Most of the various physical circumstances that emerge in the real world, especially heat and mass transfer occurrences under diverse effects, are well recognized to involve highly non-linear ODEs. These equations are complicated to solve analytically, and when this is not possible, relevant numerical methods such as the shooting method, finite difference, and other methodologies must be used. But, the differential transform method (DTM) is renowned to be one of the most appropriate methods for solving these nonlinear differential equations. This technique has the added benefit of not requiring the differential equation to be discretized, linearized, or perturbed. The finite Taylor series and the iteration operation described by the transformed equations derived from the original equation employing differential transformation operations can be utilized to assess the approximating solution. Several authors used the DTM concept to solve various types of equations [21–25]. Also, Weighted Residuals Methods (WRMs) are approximation approaches for simulating the continuation and Least Square Method (LSM) is pronounced as maximum convenient technique among the WRMs for solving the ODEs. Thus, Aziz and Bouaziz [26] employed the LSM for solving the highly nonlinear ODE of the straight fin problem. For the porous fin, Hatami et al. [27] used the LSM technique for solving the nonlinear energy equation. Furthermore, this technique is implemented in determining the solution for the heat transfer and fluid flow problems [28–30].

The literature inspection reveals that the majority of the literary work discloses the analysis of heat transfer through various structured fins such as longitudinal, radial, annular, and among several others. Besides, there is a research gap in presenting the heating pattern in longitudinal fins, particularly the implementation of analytical scheme that pronounced the effect of inclination on the surface. However, using numerical techniques, few studies (Gireesha and Sowmya [23] and Gireesha et al. [31]) have reported the effect of the inclination on the thermal distribution of fins, which is significant in energy storage applications (Yazici et al. [32] and Bouzennada et al. [33]). According to the authors' knowledge, the present study provides the approximate analytical solution for the fin problem with the impact of inclination. Thus, the novelty of this study is that examining the impact of different angles of inclination on the radiated flow of heat transmission problem of a porous straight fin with Rosseland theory and internal phenomenon of heating generation. Furthermore, the primary objective of the presented analysis is to find out the close form simulations for heating problem in longitudinal porous fin with implementation of DTM-Pade framework and LSM.

2. Mathematical formulation

The thermal flow in longitudinal fin with porous space containing the specific angle α on the surface has been conducted as presented in Fig. 1. The cross-section area of fin is assumed to be uniform. Let L , W and t length, width and thickness of porous fin, respectively. The surface temperature of porous fin is expressed with T_b while T_∞ be surrounding temperature.

Following Ndlovu and Moitsheki [16], Hatami et al. [27], the governing expression for fin configuration is:

$$q_x - q_{x+dx} = \dot{m}c_p(T - T_\infty) + (1-\varphi)h^*P(T - T_\infty) + P\varepsilon\sigma\left(T^4 - T_\infty^4\right) - A_b(1-\varphi)q^*_{\text{int}}(T) \tag{1}$$

The energy flux relation near base fin is:

$$q_b = q_{cond} + q_{rad} \tag{2}$$

The first term of R.H.S is mathematically addressed as (Kiwan [34])

$$q_{cond} = -k^* A_b \frac{dT}{dx} \tag{3}$$

where, $k^* = k_f\,\varphi + k_s(1-\varphi)$ is the thermal conductivity of the porous fin.

Following the Rosseland approximation:

$$q_{rad} = -\frac{4\sigma A_b}{3\beta_R^*}\frac{dT^4}{dx} \tag{4}$$

The expression for highlighting the flow rate via porous space is

$$\dot{m} = \rho_f u(x) W dx \tag{5}$$

The Darcy relation is

$$u(x) = \frac{g\,K\,\beta\sin(\alpha)}{\nu_f}(T - T_\infty) \tag{6}$$

Now, Eq. (1) can be written as:

$$-\frac{dq_b}{dx} - \frac{\rho_f\,c_{pf}\,g\,K\,\beta W\sin(\alpha)}{\nu_f}(T-T_\infty)^2 - (1-\varphi)h^* P(T-T_\infty) - P\varepsilon^*\sigma\left(T^4 - T_\infty^4\right) + A_b(1-\varphi)q_{\text{int}}^*(T) = 0 \tag{7}$$

The representation of heat balance expression in view of Eqs. (3)–(6) is [34]:

$$\frac{d}{dx}\left[k_f\,\varphi + k_s(1-\varphi)A_b\frac{dT}{dx}\right] + \frac{4\sigma A_b}{3\beta_R^*}\frac{d}{dx}\left[\frac{dT^4}{dx}\right] - \frac{\rho_f\,c_{pf}\,g\,K\,\beta W\sin(\alpha)}{\nu_f}(T-T_\infty)^2 - (1-\varphi)h^* P(T-T_\infty) - P\varepsilon^*\sigma\left(T^4 - T_\infty^4\right) + A_b(1-\varphi)q_{\text{int}}^*(T) = 0 \tag{8}$$

The low temperature gradient assumptions are taken into consideration, the radiative analysis is computed. The expansion of T^4 leads to Ref. [34].

$$T^4 \cong 4T_\infty^3 T - 3T_\infty^4 \tag{9}$$

Defining relation between $q_{\text{int}}^*(T)$ and $h^*(T)$ [15]:

$$q_{\text{int}}^*(T) = q_0[1 + c(T - T_\infty)],$$

$$h^*(T) = h_b\left[\frac{T-T_\infty}{T_b - T_\infty}\right]^n \tag{10}$$

With boundary assumptions [15]:

$$T(L) = T_b,$$

$$\left.\frac{dT}{dx}\right|_{x=0} = 0. \tag{11}$$

With dimensionless factors:

$$\theta(x) = \frac{T-T_\infty}{T_b - T_\infty},\ X = \frac{x}{L},\ Nc = \frac{h_b PL^2}{A_b k_s},\ S_H = \frac{RaDa}{k_S} = \frac{\rho c_p g K\beta L^2 W(T_b - T_\infty)}{\nu_f k_s A_b},\ Nr = \frac{4\sigma\varepsilon^* T_\infty^3 PL^2}{k_s A_b},\ k_r = \frac{k_f}{k_s},\ R_d^* = \frac{4\sigma T_\infty^3}{3\beta_R^* k_s},\ \gamma = c(T_b - T_\infty),$$
$$Q = \frac{q_0\,L^2}{(T_b - T_\infty)k_s}. \tag{12}$$

Using Eq. (12), Eq. (8) yields: $$\frac{d}{dX}\left[(k_r\,\varphi + (1-\varphi))\frac{d\theta}{dX}\right] + 4R_d^*\frac{d^2\theta}{dX^2} - S_H\sin(\alpha)\theta^2 - (1-\varphi)Nc\,\theta^{n+1} - Nr\,\theta + (1-\varphi)Q(1+\gamma\,\theta) = 0 \tag{13}$$

alongwith:

$$\theta(1)=1,$$

$$\left.\frac{d\theta}{dX}\right|_{X=0}=0 \tag{14}$$

3. DTM and LSM employment

3.1. DTM

The function $X(\upsilon)$ in term of $\chi(\nu)$ is characterized (see Christopher et al. [35]):

$$X(\upsilon)=\frac{1}{\upsilon!}\left[\frac{d^{\upsilon}\chi(\nu)}{dx^{\upsilon}}\right]_{\nu=\nu_0} \tag{15}$$

Let us express the differential inverse relation for $X(\upsilon)$:

$$\chi(\nu)=\sum_{\upsilon=0}^{\infty}X(\upsilon)(\nu-\nu_0)^{\upsilon} \tag{16}$$

Incorporating Eqs. (15) and (16), yields

$$\chi(l)=\sum_{\upsilon=0}^{\infty}\frac{(\nu-\nu_0)^{\upsilon}}{\upsilon!}\left[\frac{d^{\upsilon}\chi(l)}{dx^{\upsilon}}\right]_{\nu=\nu_0} \tag{17}$$

Padé approximation in the more convent analytical mechanism which based on the coefficient of power series expressions [36,37]. This approximation can tackle the higher order problems even for infinite domain successfully [38].

3.2. LSM (Least Square Method)

The LSM is based on the WRMs solver for computing the approximations for differential system [26]. The utilizing the differential operator D with function ω resulting the new function g as follows:

$$D(\omega(x))=g(x) \tag{18}$$

The relation between ω and $\widetilde{\omega}$ is defined as:

$$\omega\cong\widetilde{\omega}=\sum_{k=1}^{n}v_k\chi_k \tag{19}$$

where v_k are the unknown constants. The residual $\Upsilon(x)$ is expressed as:

$$\Upsilon(x)=D(\widetilde{\omega}(x))-g(x)\neq 0 \tag{20}$$

Now

$$\int_X \Upsilon(x)\,H_k(x)dx=0 \quad k=1,\ 2,\ldots.n \tag{21}$$

It is remarked that the approximation between H_k and v_k in ω are equal. For minimum squared residuals, one get:

$$M=\int_X \Upsilon(x)\ \Upsilon(x)dx=\int_X \Upsilon^2(x)\,dx \tag{22}$$

For assumption of low scalar function, the derivative of M for unknown constants should be zero.

$$\frac{\partial M}{\partial v_k}=2\int_X \Upsilon(x)\ \frac{\partial \Upsilon}{\partial v_k}dx=0 \tag{23}$$

Equating with Eq. (21), H_k can be:

$$H_k=2\frac{\partial \Upsilon}{\partial v_k} \tag{24}$$

which gets:

$$H_k=\frac{\partial \Upsilon}{\partial v_k} \tag{25}$$

4. Implementation of LSM and DTM-Pade technique

4.1. LSM operation

The implementation of LSM for thermal distribution in view of conditions (14) is:

$$\theta(X) = 1 + A\left(1 - X^2\right) + B\left(1 - X^3\right) + \Gamma\left(1 - X^4\right) \tag{26}$$

The relation for residual function in view of Eq. (13) is:

$$\begin{aligned}\Psi(A,B,\Gamma,X) = {} & -2S_H \sin(\alpha)A - S_H \sin(\alpha)A^2 - S_H \sin(\alpha)B^2 - S_H \sin(\alpha)\Gamma^2 - 2S_H \sin(\alpha)B - 2S_H \sin(\alpha)\Gamma + \\ & 12\Gamma\varphi X^2 - 2Ak_r\varphi + 6B\varphi X - 48\Gamma R_d^* X^2 - 24BR_d^* X + \Gamma NrX^4 + BNrX^3 + ANrX^2 + AQ\gamma + BQ\gamma + \Gamma Q\gamma - Q\gamma\varphi - \\ & 2S_H \sin(\alpha)ABX^5 + 2S_H \sin(\alpha)A\Gamma X^4 + 2S_H \sin(\alpha)B\Gamma X^4 + 2S_H \sin(\alpha)ABX^3 + 2S_H \sin(\alpha)B\Gamma X^3 + \\ & 2S_H \sin(\alpha)ABX^2 + 2S_H \sin(\alpha)A\Gamma X^2 + \Gamma Q\gamma\varphi X^4 + BQ\gamma\varphi X^3 + AQ\gamma\varphi X^2 - 2S_H \sin(\alpha)B\Gamma X^7 - 2S_H \sin(\alpha)A\Gamma X^6 - \\ & \Gamma Nc\varphi X^4 - BNc\varphi X^3 - ANc\varphi X^2 - S_H \sin(\alpha)\Gamma^2 X^8 - S_H \sin(\alpha)B^2 X^6 - S_H \sin(\alpha)A^2 X^4 + 2S_H \sin(\alpha)\Gamma^2 X^4 + \\ & 2S_H \sin(\alpha)B^2 X^3 + 2S_H \sin(\alpha)\Gamma X^4 + 2S_H \sin(\alpha)A^2 X^2 + 2S_H \sin(\alpha)BX^3 + 2S_H \sin(\alpha)AX^2 - 2S_H \sin(\alpha)AB - \\ & 2S_H \sin(\alpha)A\Gamma - 2S_H \sin(\alpha)B\Gamma - 12\Gamma k_r\varphi X^2 - 6Bk_r\varphi X - \Gamma Q\gamma X^4 - BQ\gamma X^3 - AQ\gamma X^2 - AQ\gamma\varphi - BQ\gamma\varphi - \\ & \Gamma Q\gamma\varphi - S_H \sin(\alpha) + Q - 12\Gamma X^2 - 6BX - Nr - Nc - 2A + ANcX^2 + \Gamma Nc\varphi + BNc\varphi + ANc\varphi + \Gamma NcX^4 + BNcX^3 - \\ & A\,Nc - BNc - \Gamma\,Nc + Nc\,\varphi + 2\,A\varphi - 8\,AR_d^* - ANr - BNr - \Gamma Nr + Q\,\gamma - Q\,\varphi\end{aligned} \tag{27}$$

Upon replacing the residual function in Eq. (21) with coefficients A, B and Γ are obtained by simulating the coupled systems. Inserting the obtained values in Eq. (26) yields:

$$\theta(X) = 0.6582798778 + 0.3069098528X^2 - 0.004554954116X^3 + 0.03936522345X^4 \tag{28}$$

4.2. Applications of DTM-Pade approximant

Using the differential transform for Eqs. 13 and 14 yield:

$$\begin{aligned}&(1 - \varphi + k_r\varphi)(S+1)(S+2)\theta[S+2] + 4R_d^*(S+1)(S+2)\theta[S+2] - S_H \sin(\alpha)\sum_{\ell=0}^{S}\theta[S-\ell]\theta[\ell] \\ &-(1-\varphi)Nc\,\theta[S] - Nr\,\theta[S] + (1-\varphi)Q(\gamma\,\theta[S] + \delta[S]) = 0\end{aligned} \tag{29}$$

$$\theta[0] = A,\ \theta[1] = 0 \tag{30}$$

with constant A.

The recurrence relation for S is:

$$\theta[2] = \frac{1}{2\left(k_r\varphi + 4R_d^* - \varphi + 1\right)}\left[S_H \sin(\alpha)A^2 + AQ\gamma\varphi - NcA\varphi - AQ\gamma + NcA + NrA + Q\varphi - Q\right] \tag{31}$$

$$\theta[3] = 0 \tag{32}$$

$$\theta[4] = \frac{1}{24\left(k_r\varphi + 4R_d^* - \varphi + 1\right)^2}\begin{bmatrix} 2NcANr - Q\varphi^2 Nc + AQ^2\gamma^2 + 2Q\varphi Nc - 2Nc^2 A\varphi + Q\varphi Nr + Q^2\varphi^2\gamma - 2Q^2\varphi\gamma + \\ Nc^2 A\varphi^2 + 2(S_H)^2 \sin(\alpha)^2 A^3 - 3S_H \sin(\alpha)A^2 Nc\varphi - 3S_H \sin(\alpha)A^2 Q\gamma - \\ 2AQ\gamma\varphi^2 Nc + 4AQ\gamma\varphi Nc + 2AQ\gamma\varphi Nr + 2Q\varphi S_H \sin(\alpha)A + Nc^2 A + \\ Nr^2 A + Q^2\gamma - QNc - QNr + 3S_H \sin(\alpha)A^2 Q\gamma\varphi + 3S_H \sin(\alpha)A^2 Nc + \\ 3S_H \sin(\alpha)A^2 Nr + AQ^2\gamma^2\varphi^2 - 2AQ^2\gamma^2\varphi - 2NcA\varphi Nr - 2AQ\gamma Nc - \\ 2AQ\gamma Nr - 2QS_H \sin(\alpha)A \end{bmatrix} \tag{33}$$

Table 1
The operators of DTM.

Original function	Transformed function
$\chi(\nu) = z_1(\nu) \pm z_2(\nu)$	$X(\upsilon) = Z_1(\upsilon) \pm Z_2(\upsilon)$
$\chi(\nu) = m\, z(\nu)$	$X(\upsilon) = mZ(\upsilon)$, where m is the constant.
$\chi(\nu) = \frac{d\, z(\nu)}{d\nu}$	$X(\upsilon) = (\upsilon+1)Z(\upsilon+1)$
$\chi(\nu) = \frac{d^{\,p} z(\nu)}{d\nu}$	$X(\upsilon) = (\upsilon+1)(\upsilon+1)...(\upsilon+n)Z(\upsilon+p)$
$\chi(\nu) = \nu^m$	$X(\upsilon) = \delta(\upsilon - m) = \begin{cases} 1, & \upsilon = m \\ 0, & \upsilon \neq m \end{cases}$
$\chi(\nu) = z_1(\nu) z_2(\nu)$	$X(\upsilon) = \sum_{r=0}^{\upsilon} Z_1(r) Z_2(\upsilon - r)$
$\chi(\nu) = z_1(\nu) z_2(\nu) .... \ldots..z_{s-1}(\nu) z_s(\nu)$	$X(\upsilon) = \sum_{\upsilon_{s-1}=0}^{\upsilon} \sum_{\upsilon_{s-2}=0}^{\upsilon_{s-1}=0} .... \sum_{\upsilon_2=0}^{\upsilon_3} \sum_{\upsilon_1=0}^{\upsilon_2} Z_1(\upsilon_1)\, Z_2(\upsilon_2 - \upsilon_1)..Z_{s-1}(\upsilon_{s-1} - \upsilon_{s-2}) Z_s(\upsilon - \upsilon_{s-1})$

Table 2
Comparative change in $\theta(X)$ for $Nc = 1$, $\gamma = 0.1$, $S_H = 0.7$, $Nr = 1$, $Q = 0.8$, $R_d^* = 0.3$, $\varphi = 0.1$, and $k_r = 0.1$.

X		0	0.1	0.2	0.3	0.4
$\alpha = 30^0$	**NM**	0.76817	0.77028	0.77664	0.78732	0.80245
	DTM	0.76755	0.76966	0.77601	0.78667	0.80177
	LSM	0.76818	0.77030	0.77668	0.78738	0.80251
$\alpha = 90^0$	**NM**	0.73437	0.73674	0.74389	0.75591	0.77296
	DTM	0.73355	0.73592	0.74305	0.75504	0.77206
	LSM	0.73439	0.73678	0.74395	0.75600	0.77309

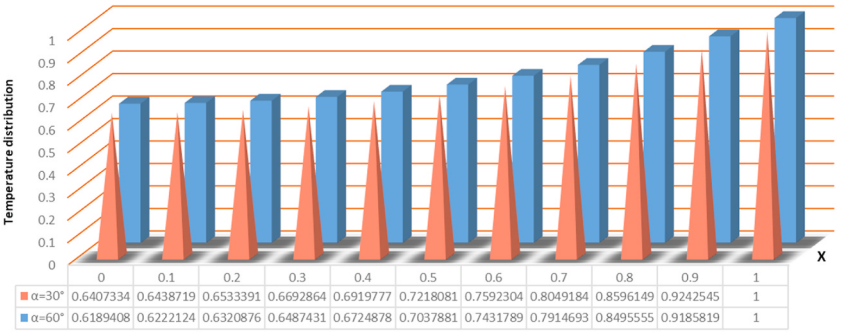

Fig. 2. Temperature distribution against fin's length.

and so on. Using equations (30)-(33), we get:

$$\theta(x) = A + \left[\frac{1}{2\left(k_r\varphi + 4R_d^* - \varphi + 1\right)}\left(S_H \sin(\alpha)A^2 + AQ\gamma\varphi - NcA\varphi - AQ\gamma + NcA + NrA + Q\varphi - Q\right)\right]X^2 +$$

$$\left[\frac{1}{24\left(k_r\varphi + 4R_d^* - \varphi + 1\right)^2}\left(\begin{array}{l} 2NcANr - Q\varphi^2 Nc + AQ^2\gamma^2 + 2Q\varphi Nc - 2Nc^2A\varphi + Q\varphi Nr + Q^2\varphi^2\gamma - 2Q^2\varphi\gamma + \\ Nc^2A\varphi^2 + 2(S_H)^2 \sin(\alpha)^2A^3 - 3S_H \sin(\alpha)A^2Nc\varphi - 3S_H \sin(\alpha)A^2Q\gamma - \\ 2AQ\gamma\varphi^2Nc + 4AQ\gamma\varphi Nc + 2AQ\gamma\varphi Nr + 2Q\varphi S_H \sin(\alpha)A + Nc^2A + \\ Nr^2A + Q^2\gamma - QNc - QNr + 3S_H \sin(\alpha)A^2Q\gamma\varphi + 3S_H \sin(\alpha)A^2Nc + \\ 3S_H \sin(\alpha)A^2Nr + AQ^2\gamma^2\varphi^2 - 2AQ^2\gamma^2\varphi - 2NcA\varphi Nr - 2AQ\gamma Nc - \\ 2AQ\gamma Nr - 2QS_H \sin(\alpha)A \end{array}\right)\right]X^4 + ... \quad (34)$$

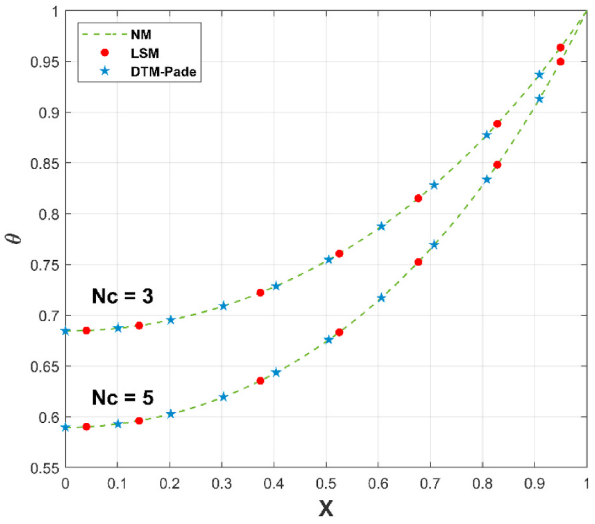

Fig. 3. Validation of the present problem.

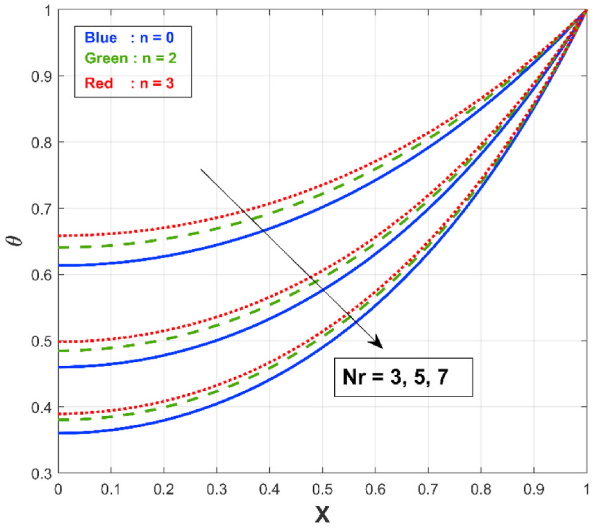

Fig. 4. Upshot of *Nr* on θ.

Utilizing the Padé framework on Eq. (34), the numerical value of Λ is measured to be $\Lambda = 0.65684$. $Nc = 3, \gamma = 0.1, S_H = 0.5$, $Nr = 1, Q = 0.8, R_d^* = 0.5, \varphi = 0.1, k_r = 0.1$ and $\alpha = 30^0$ are inserted in Eq. (34), to obtained [39–43]:

$$\theta(X) = 0.6568438418 + 0.3042767037X^2 + 0.03447442787X^4 + \ldots \tag{35}$$

5. Results and discussions

The current investigation present the exploration of temperature difference associated due to internal heating phenomenon via porous inclined longitudinal fin. The achieved ODE is solved via DTM and LSM algorithm after non-dimensionalizing the heat expression (equation) with dimensionless terms (Table 1). The insight impact of parameters like porosity factor S_H, radiation-conduction R_d^*, heat generation constant Q, radiation number Nr, angle of inclination α, and convection-conduction parameter Nc, results mainly referred to temperature field and thermal profile rate are depicted. Since this model is based on thermal flow assumptions, so the graphical simulations are performed for the specified range of flow parameters like $3 \leq Nr \leq 9, 0.3 \leq R_d^* \leq 0.9, 2 \leq Nc \leq 4, 0 \leq Q \leq 0.9, 0.5 \leq S_H \leq 0.9$. Table 2 find out the DTM and LSM presentation with numerical outcomes with excellent manner.

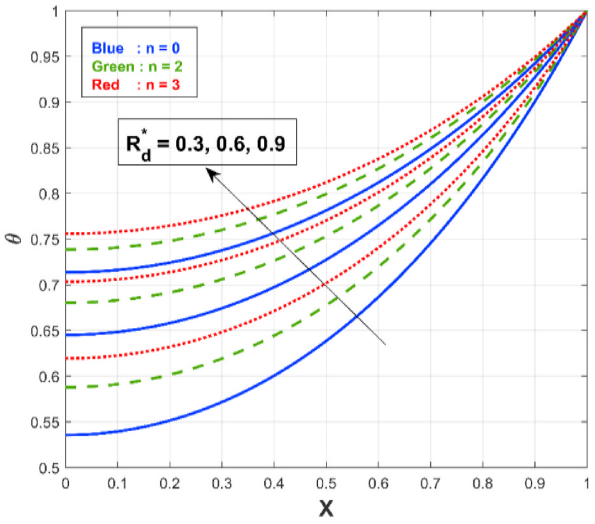

Fig. 5. Behavior of R_d^* on θ.

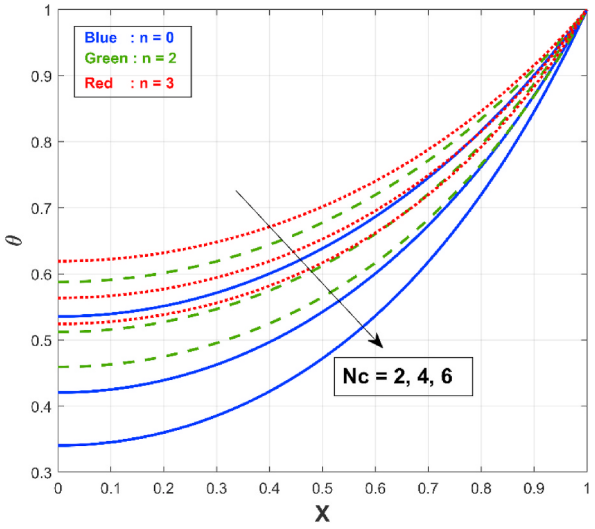

Fig. 6. Behavior of *Nc* on θ.

Fig. 2 shows the nature of thermal distribution from the fin's base to its tip via convective and radiative heat transfer on the surface of the fin for $\alpha = 30^0$ and $\alpha = 60^0$. The corresponding numerical values of temperature field for equally spaced locations of the fin length are also presented. From this figure, it is confirmed that the temperature varies in decreasing manner from base to top of fin. The verification of results via DTM and LSM approach have been done in Fig. 3, and the accomplished outcomes have admirable convergence with the computational results. For constant $(n = 0)$, nucleate boiling $(n = 2)$, and radiation $(n = 3)$ modes of heat transfer, the radaitve parameter impact is explained in Fig. 4. With an increment in the radiation number, the thermal profile θ decreases steadily. The lower temperature inside the fin indicates a loss of ambient fluid temperature with radiative parameter. The thermal outcomes with radiative constant enhanced the heating transmission from the fin, according to the results. The dispersion of temperature is higher for $n = 3$ than other two modes. Fig. 5 pronounced the temperature rate as a result of the R_d^* for the

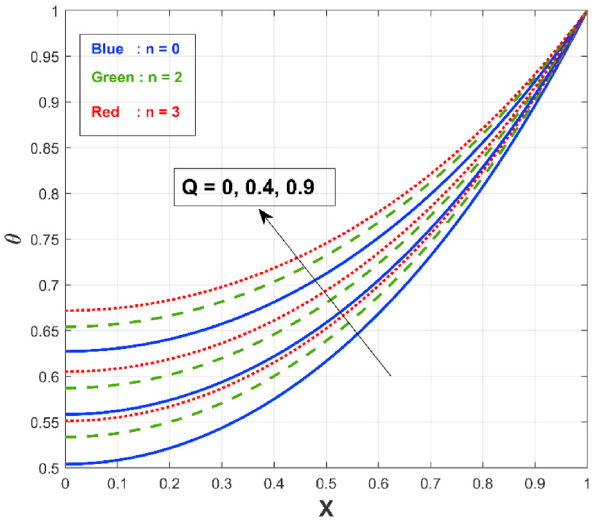

Fig. 7. Behavior of Q on θ.

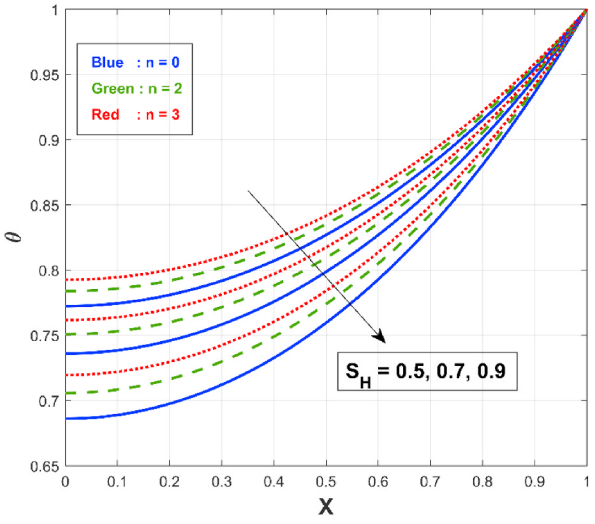

Fig. 8(a). Behavior of S_H on θ.

aforementioned mode of heat transfer. The thermal distribution through the fin increases which is caused by an upsurge in the scale of R_d^*, as shown in this figure.

For minimal change in radiation-conduction constant, heat transfer via convection dominates; however, as the R_d^* rises, heat transfer via radiation takes over. Upon encasing the energy flux, the temperature of the fin. Also, θ is gradually higher for $n = 3$ than $n = 0$ and $n = 2$. Fig. 6 showed the influence of the Nc on the thermal attribute of the porous fin. The thermal profile through the fin is declined in this figure by increasing the *Nc*. As this parameter intensifies, the enriched heating patter in fin is noted which declined the temperature rise. A dropping scene in fin temperature is noted while progressive change in temperature is observed through fin base. The contribution of this flow parameter is important to enhancing the thermal transport of fin. Moreover, θ exhibits increased behavior for $n = 3$ than other two modes of heat transfer. The temperature profile of the fin is shown in Fig. 7 as a result of the internal heat generation parameter. As Q value improves, the thermal distribution of the fin strengthens. The improved change in this flow parameter enhanced the heat generation via the fin. Subsequently, improving the heating generation raises the temperature profile. Higher heat generation enhances fin temperature in steady-state conditions owing to fact of larger dissipation of heating environment due to fin. The significance of S_H on the temperature field of the fin for various heat transfer mechanisms is demonstrated in Fig. 8(a).

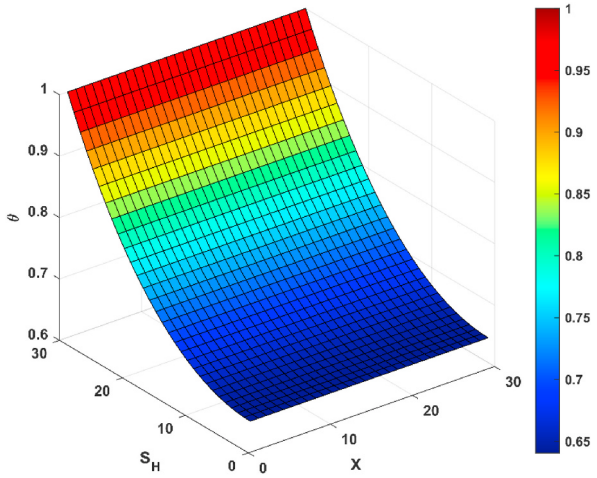

Fig. 8(b). 3D illustration of S_H on θ.

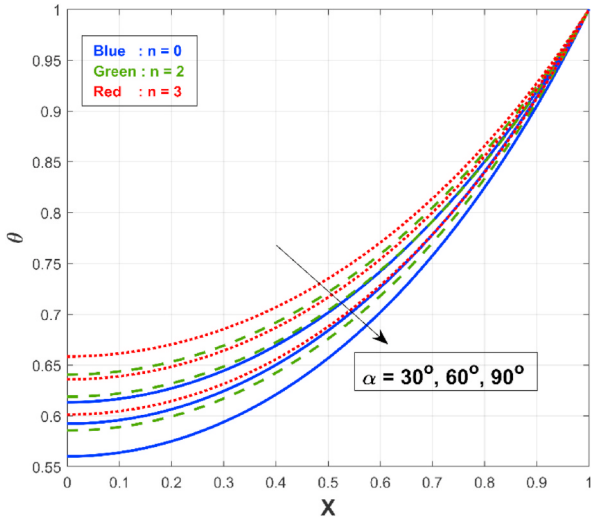

Fig. 9(a). Upshot of α on θ.

With enrich change in porosity constant, the fin thermal measurement reduces. The same behavior can be seen in Fig. 8(b) in a three-dimensional (3D) illustration. The main factor for this is that with making increment in porosity factor, the porous cool down with rapid rate and later on attain the ambient heating constraints. Higher thermal variation is noticed for $n = 3$ than other two modes of heat transfer. Fig. 9(a)–9(d) portrays the consequence of the angle of inclination on the thermal behavior of the fin. It has been noticed that as the tilt angle increases ($\alpha = 30^0, 60^0, 90^0$), the temperature of the fins diminishes (see Fig. 9(a)). This is because of the driving force for convection, which is magnified by the angle of inclination. The 3D representation indicating the effect of inclination on thermal profile is presented in Fig. 9(b)–9(d). Similar nature as seen in Fig. 9(a) is noticed here for $\alpha = 30^0, 45^0, 60^0$.

6. Final remarks

The framework for temperature rate is presented via inclined porous longitudinal fin subject to the internal heating applications. The Rosseland theory is used to determine the features of radiative phenomenon. The LSM and DTM-Pade approximations are followed for simulation process. Graphical explanations are manifested for the consequence of parameters in heat transfer of porous fin. The key findings of this analysis are as follows:

- ❖ Upon enhancing the convection-conduction parameter, the thermal dispersal in the fin lowers.
- ❖ The thermal profile inside the fin declines as the porosity factor rises.
- ❖ A more strengthens heat trnasfer via porous fine is observed for radiative-conduction constant.

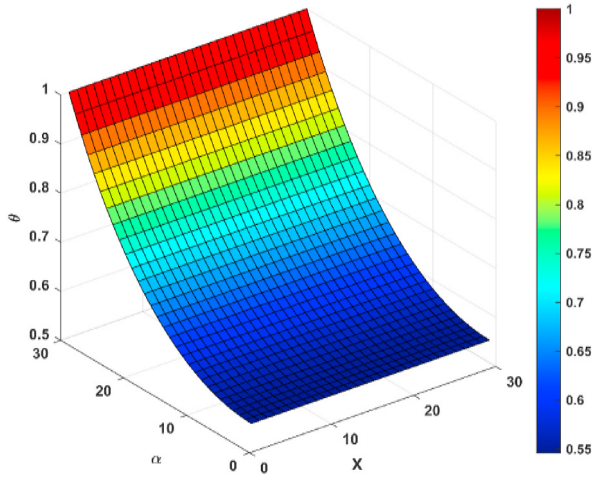

Fig. 9(b). 3D illustration of θ for $\alpha = 30^0$.

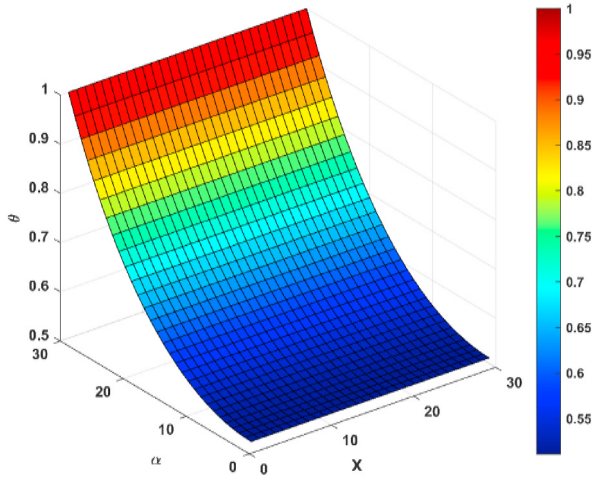

Fig. 9(c). 3D illustration of θ for $\alpha = 45^0$.

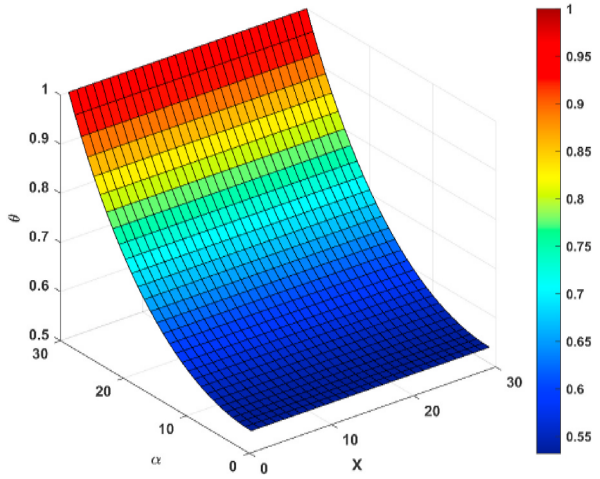

Fig. 9(d). 3D illustration of θ for $\alpha = 60^0$.

- ❖ The angle of inclination greatly influences the thermal capacity of fine. When is inclined to an escalating angle, the thermal behavior of the fin declines.
- ❖ The thermal rate of porous fine improves with augmented change of heat-generating parameter.
- ❖ This scrutiny convince that DTM-Pade and LSM alogrithms are effecinet and convenient methods for nonlinear differentail systems.
- ❖ The obtained result can be further extended for hybird nnaolfuid, modifed hybrid nnaofluid and by utilizing various thermal consequences like entropy generation, nonlinear radiatve analysis, stabilty analysis, activation energy, non-uniform heat source/sink and thermo-diffsuion feautres.

Declaration of competing interest

The authors declare that they have no known competing financial interests or personal relationships that could have appeared to influence the work reported in this paper.

Acknowledgements

The authors extend their appreciation to the Deanship of Scientific Research at King Khalid University, Abha 61413, Saudi Arabia for funding this work through research groups program under grant number R.G.P-2-110-1443.

References

[1] V. Kumar, J.K. Madhukesh, A.M. Jyothi, B.C. Prasannakumara, M. Ijaz Khan, Y.-M. Chu, Analysis of single and multi-wall carbon nanotubes (SWCNT/MWCNT) in the flow of Maxwell nanofluid with the impact of magnetic dipole, Comput. Theor. Chem. 1200 (Jun. 2021), 113223, https://doi.org/10.1016/j.comptc.2021.113223.
[2] M. Veera Krishna, N. Ameer Ahamad, Ali J. Chamkha, Radiation absorption on MHD convective flow of nanofluids through vertically travelling absorbent plate, Ain Shams Eng. J. 12 (3) (September 2021) 3043–3056.
[[3]] M. Veera Krishna, N. Ameer Ahamad, A.F. Aljohani, Thermal radiation, chemical reaction, Hall and ion slip effects on MHD oscillatory rotating flow of micro-polar liquid, Alex. Eng. J. 60 (3) (June 2021) 3467–3484.
[[4]] N. Ameer Ahamad, Azeem, Maughal Ahmed Ali Baig, Sarfaraz Kamangar, Irfan Anjum Badruddin, Jana Nagarjun, Heat transfer in square porous cavity due to radiation and heat generating strip - Part II, Conf. Ser.: Mater. Sci. Eng. 764 (2020), 012030.
[5] J. Madhukesh, B. Prasannakumara, R. V. Kumar, A. Rauf, and S. Shehzad, "Flow of hydromagnetic Micropolar-Casson nanofluid over porous disks influenced by Cattaneo-Christov theory and slip effects," J. Porous Media, doi: 10.1615/JPorMedia.2021039254.
[6] D.U. Sarwe, B. Shanker, R. Mishra, R.V. Kumar, M.R. Shekar, Simultaneous impact of magnetic and Arrhenius activation energy on the flow of Casson hybrid nanofluid over a vertically moving plate, Int J Thermofluid Sci Technol 8 (2021).
[7] N. Abbas, S. Nadeem, A. Saleem, M.Y. Malik, A. Issakhov, F.M. Alharbi, Models base study of inclined MHD of hybrid nanofluid flow over nonlinear stretching cylinder, Chin. J. Phys. 69 (Feb. 2021) 109–117, https://doi.org/10.1016/j.cjph.2020.11.019.
[8] J. Madhukesh, A. Alhadhrami, R. Naveen Kumar, R. Punith Gowda, B. Prasannakumara, R. Varun Kumar, Physical insights into the heat and mass transfer in Casson hybrid nanofluid flow induced by a Riga plate with thermophoretic particle deposition, Proc. Inst. Mech. Eng. Part E J. Process Mech. Eng. (Aug. 2021), https://doi.org/10.1177/09544089211039305, 09544089211039305.
[9] A. Hamid, R. Naveen Kumar, R.J. Punith Gowda, R.S. Varun Kumar, S.U. Khan, M. Ijaz Khan, B.C. Prasannakumara, T. Muhammad, Impact of Hall current and homogenous–heterogenous reactions on MHD flow of GO-MoS2/water (H2O)-ethylene glycol (C2H6O2) hybrid nanofluid past a vertical stretching surface, Waves Random Complex Media (Oct. 2021) 1–18, https://doi.org/10.1080/17455030.2021.1985746, 0, no. 0.
[10] J. K. Madhukesh, R. S. Varun Kumar, R. J. Punith Gowda, B. C. Prasannakumara, and S. A. Shehzad, "Thermophoretic particle deposition and heat generation analysis of Newtonian nanofluid flow through magnetized Riga plate," Heat Transf., vol. n/a, no. n/a, doi: 10.1002/htj.22438.
[11] M. Turkyilmazoglu, Heat transfer from moving exponential fins exposed to heat generation, Int. J. Heat Mass Tran. 116 (Jan. 2018) 346–351, https://doi.org/10.1016/j.ijheatmasstransfer.2017.08.091.
[12] P.L. Ndlovu, R.J. Moitsheki, Analysis of transient heat transfer in radial moving fins with temperature-dependent thermal properties, J. Therm. Anal. Calorim. 138 (4) (Nov. 2019) 2913–2921, https://doi.org/10.1007/s10973-019-08306-5.
[13] G. Sowmya, B.J. Gireesha, H. Berrehal, An unsteady thermal investigation of a wetted longitudinal porous fin of different profiles, J. Therm. Anal. Calorim. 143 (3) (Feb. 2021) 2463–2474, https://doi.org/10.1007/s10973-020-09963-7.
[14] M. Fallah Najafabadi, H. Talebi Rostami, K. Hosseinzadeh, D. Domiri Ganji, Thermal analysis of a moving fin using the radial basis function approximation, Heat Transf 50 (8) (2021) 7553–7567, https://doi.org/10.1002/htj.22242.
[15] M.C. Jayaprakash, Hassan A.H. Alzahrani, G. Sowmya, R.S. Varun Kumar, M.Y. Malik, Abdulmohsen Alsaiari, B.C. Prasannakumara, Thermal distribution through a moving longitudinal trapezoidal fin with variable temperature-dependent thermal properties using DTM-Pade approximant, Case Stud. Therm. Eng. 28 (Dec. 2021), 101697, https://doi.org/10.1016/j.csite.2021.101697.
[16] P.L. Ndlovu, R.J. Moitsheki, Steady state heat transfer analysis in a rectangular moving porous fin, Propuls. Power Res. 9 (2) (Jun. 2020) 188–196, https://doi.org/10.1016/j.jppr.2020.03.002.
[17] G. Sowmya, B.J. Gireesha, Thermal stresses and efficiency analysis of a radial porous fin with radiation and variable thermal conductivity and internal heat generation, J. Therm. Anal. Calorim. (May 2021), https://doi.org/10.1007/s10973-021-10801-7.
[18] B. Kundu, S.-J. Yook, An accurate approach for thermal analysis of porous longitudinal, spine and radial fins with all nonlinearity effects – analytical and unified assessment, Appl. Math. Comput. 402 (Aug. 2021), 126124, https://doi.org/10.1016/j.amc.2021.126124.
[19] G. Sowmya, B.J. Gireesha, Analysis of heat transfer through different profiled longitudinal porous fin by differential transformation method, Heat Transf 51 (2) (2022) 2165–2180, https://doi.org/10.1002/htj.22394.
[20] R. Das, B. Kundu, Simultaneous estimation of heat generation and magnetic field in a radial porous fin from surface temperature information, Int. Commun. Heat Mass Tran. 127 (Oct. 2021), 105497, https://doi.org/10.1016/j.icheatmasstransfer.2021.105497.
[21] A. Moradi, T. Hayat, A. Alsaedi, Convection-radiation thermal analysis of triangular porous fins with temperature-dependent thermal conductivity by DTM, Energy Convers. Manag. 77 (Jan. 2014) 70–77, https://doi.org/10.1016/j.enconman.2013.09.016.
[22] P.L. Ndlovu, Analytical study of transient heat transfer in a triangular moving porous fin with temperature dependant thermal properties," defect diffus, Forum 393 (2019) 31–46. www.scientific.net/DDF.393.31.
[23] B.J. Gireesha, G. Sowmya, Heat transfer analysis of an inclined porous fin using Differential Transform Method, Int. J. Ambient Energy (Sep. 2020) 1–7, https://doi.org/10.1080/01430750.2020.1818619, 0, no. 0.
[24] H. Abbasi, A. Javed, Implementation of differential transform method (DTM) for large deformation analysis of cantilever beam, IOP Conf. Ser. Mater. Sci. Eng. 899 (1) (Jul. 2020), https://doi.org/10.1088/1757-899X/899/1/012003, 012003.
[25] G.İ. Aksoy, Application of differential transformation method for an annular fin with variable thermal conductivity, Therm. Sci. (2021), 00, pp. 315–315.
[26] A. Aziz, M.N. Bouaziz, A least squares method for a longitudinal fin with temperature dependent internal heat generation and thermal conductivity, Energy Convers. Manag. 52 (8) (Aug. 2011) 2876–2882, https://doi.org/10.1016/j.enconman.2011.04.003.

[27] M. Hatami, A. Hasanpour, D.D. Ganji, Heat transfer study through porous fins (Si3N4 and AL) with temperature-dependent heat generation, Energy Convers. Manag. 74 (Oct. 2013) 9–16, https://doi.org/10.1016/j.enconman.2013.04.034.
[28] M. Hatami, D.D. Ganji, Thermal and flow analysis of microchannel heat sink (MCHS) cooled by Cu–water nanofluid using porous media approach and least square method, Energy Convers. Manag. 78 (Feb. 2014) 347–358, https://doi.org/10.1016/j.enconman.2013.10.063.
[29] I. Mustafa, Z. Abbas, A. Arif, T. Javed, A. Ghaffari, Stability analysis for multiple solutions of boundary layer flow towards a shrinking sheet: analytical solution by using least square method, Phys. Stat. Mech. Its Appl. 540 (Feb. 2020), 123028, https://doi.org/10.1016/j.physa.2019.123028.
[30] U. Biswal, S. Chakraverty, B.K. Ojha, A.K. Hussein, Numerical simulation of magnetohydrodynamics nanofluid flow in a semi-porous channel with a new approach in the least square method, Int. Commun. Heat Mass Tran. 121 (Feb. 2021), 105085, https://doi.org/10.1016/j.icheatmasstransfer.2020.105085.
[31] B.J. Gireesha, M.L. Keerthi, K.M. Eshwarappa, Heat transfer analysis of longitudinal fins of trapezoidal and dovetail profile on an inclined surface, Phys. Scripta 96 (12) (Aug. 2021), 125209, https://doi.org/10.1088/1402-4896/ac1e5d.
[32] M.Y. Yazici, M. Avci, O. Aydin, Combined effects of inclination angle and fin number on thermal performance of a PCM-based heat sink, Appl. Therm. Eng. 159 (Aug. 2019), 113956, https://doi.org/10.1016/j.applthermaleng.2019.113956.
[33] T. Bouzennada, F. Mechighel, T. Ismail, L. Kolsi, K. Ghachem, Heat transfer and fluid flow in a PCM-filled enclosure: effect of inclination angle and mid-separation fin, Int. Commun. Heat Mass Tran. 124 (May 2021), 105280, https://doi.org/10.1016/j.icheatmasstransfer.2021.105280.
[34] S. Kiwan, Effect of radiative losses on the heat transfer from porous fins, Int. J. Therm. Sci. 46 (10) (Oct. 2007) 1046–1055, https://doi.org/10.1016/j.ijthermalsci.2006.11.013.
[35] A. John Christopher, N. Magesh, R.J. Punith Gowda, R. Naveen Kumar, R.S. Varun Kumar, Hybrid nanofluid flow over a stretched cylinder with the impact of homogeneous–heterogeneous reactions and Cattaneo–Christov heat flux: series solution and numerical simulation, Heat Transf 50 (4) (2021) 3800–3821, https://doi.org/10.1002/htj.22052.
[36] J.P. Boyd, Padé approximant algorithm for solving nonlinear ordinary differential equation boundary value problems on an unbounded domain, Comput. Phys. 11 (3) (May 1997) 299–303, https://doi.org/10.1063/1.168606.
[37] G. Sowmya, I.E. Sarris, C.S. Vishalakshi, R.S.V. Kumar, B.C. Prasannakumara, Analysis of transient thermal distribution in a convective–radiative moving rod using two-dimensional differential transform method with multivariate pade approximant, Symmetry 13 (10) (Oct. 2021), https://doi.org/10.3390/sym13101793. Art. no. 10.
[38] M.M. Rashidi, N. Freidoonimehr, E. Momoniat, B. Rostami, Study of nonlinear MHD tribological squeeze film at generalized magnetic Reynolds numbers using DTM, PLoS One 10 (8) (Aug. 2015), e0135004, https://doi.org/10.1371/journal.pone.0135004.
[39] M. Nazeer, F. Hussain, M.I. Khan, A.U. Rehman, E.R. El-Zahar, Y.M. Chu, M.Y. Malik, Theoretical study of MHD electro-osmotically flow of third-grade fluid in micro channel, Appl. Math. Comput. 420 (2022), 126868.
[40] Y.M. Chu, B.M. Shankaralingappa, B.J. Gireesha, F. Alzahrani, M.I. Khan, S.U. Khan, Combined impact of Cattaneo-Christov double diffusion and radiative heat flux on bio-convective flow of Maxwell liquid configured by a stretched nano-material surface, Appl. Math. Comput. 419 (2022), 126883.
[41] T.-H. Zhao, M.I. Khan, Y.-M. Chu, Artificial neural networking (ANN) analysis for heat and entropy generation in flow of non-Newtonian fluid between two rotating disks, Math. Methods Appl. Sci. (2021), https://doi.org/10.1002/mma.7310.
[42] Y.-M. Chu, U. Nazir, M. Sohail, M.M. Selim, J.-R. Lee, Enhancement in thermal energy and solute particles using hybrid nanoparticles by engaging activation energy and chemical reaction over a parabolic surface via finite element approach, Fractal Fract 5 (3) (2021) 17, https://doi.org/10.3390/fractalfract5030119. Article 119.
[43] T.-H. Zhao, O. Castillo, H. Jahanshahi, A. Yusuf, M.O. Alassafi, F.E. Alsaadi, Y.-M. Chu, A fuzzy-based strategy to suppress the novel coronavirus (2019-NCOV) massive outbreak, Appl. Comput. Math. 20 (1) (2021) 160–176.